Reaction of *Desulfovibrio vulgaris* Two-Iron Superoxide Reductase with Superoxide: Insights from Stopped-Flow Spectrophotometry†

Victor W. Huang,‡ Joseph P. Emerson,§ and Donald M. Kurtz, Jr.*,‡

Departments of Chemistry, University of Texas at San Antonio, San Antonio, Texas 78249, and University of Georgia, Athens, Georgia 30602

Received March 6, 2007; Revised Manuscript Received July 30, 2007

ABSTRACT: Stopped-flow mixing of the *Desulfovibrio vulgaris* two-iron superoxide reductase (2Fe-SOR) containing the ferrous active site with superoxide generates a dead time intermediate whose absorption spectrum is identical to that of a putative ferric−hydroperoxo intermediate previously observed by pulse radiolysis. The dead time intermediate is shown to be a product of reaction with superoxide and to be generated at a much higher proportion of active sites than by pulse radiolysis. This intermediate decays smoothly to the resting ferric active site (∼30 s^{-1} at 2 °C and pH 7) with no other detectable intermediates. Deuterium isotope effects demonstrate that solvent proton donation occurs in the rate-determining step of dead time intermediate decay and that neither of the conserved pocket residues, Glu47 or Lys48, functions as a rate-determining proton donor between pH 6 and pH 8. Fluoride, formate, azide, and phosphate accelerate decay of the dead time intermediate and for azide or fluoride lead directly to ferric−azido or −fluoro complexes of the active site, which inhibit Glu47 ligation. A solvent deuterium isotope effect is observed for the azide-accelerated decay, and the decay rate constants are proportional to the concentrations and pK_a values of HX ($X^- = F^-$, HCO_2^-, N_3^-). These data indicate that the protonated forms of the anions function analogously to solvent as general acids in the rate-determining step. The results support the notion that the ferrous SOR site reacts with superoxide by an inner sphere process, leading directly to the ferric−hydroperoxo intermediate, and demonstrate that the decay of this intermediate is subject to both specific- and general-acid catalysis.

Many air-sensitive bacteria and archaea use non-heme iron enzymes called superoxide reductases (SORs)[1] as an alternative to the classical superoxide dismutases for scavenging intracellular superoxide (*1*−*4*). The reaction catalyzed by SORs, $2H^+ + O_2^- + e^- \rightarrow H_2O_2$, occurs via reduction of superoxide by the five-coordinate ferrous [Fe(NHis)$_4$(SCys)] active site (hereafter referred to as the SOR site) according to the kinetics summarized in Scheme 1. Unlike the buried active sites in the iron-containing superoxide dismutases (*2*), the SOR sites are located at the surface of the proteins and exposed to solvent. At least two types of SORs are known:

Scheme 1

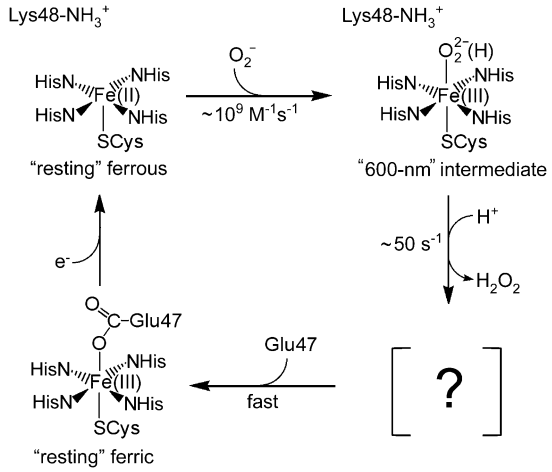

1Fe-SORs contain the SOR site as the only prosthetic group, and 2Fe-SORs contain an additional, distal [Fe(SCys)$_4$] site of unknown function. The [Fe(SCys)$_4$] site can be removed from *Desulfovibrio vulgaris* 2Fe-SOR by a single Cys → Ser mutation (C13S) with no loss of SOR function or significant alteration of the kinetics shown in Scheme 1 (*5*).

Our original studies of *D. vulgaris* 2Fe-SOR (*6*, *7*) established that the initial, diffusion-controlled encounter of the ferrous SOR site with superoxide resulted in an intermediate (λ_{max} 590−600 nm) that decayed in a superoxide-independent first-order process to the six-coordinate glutamate-

† This research was supported by U.S. National Institutes of Health Grant GM040388 (D.M.K.).

* To whom correspondence should be addressed: Phone: (210) 458-7060. Fax: (210) 458-7428. E-mail: donald.kurtz@utsa.edu.

‡ University of Texas at San Antonio.

§ University of Georgia.

[1] Abbreviations: SOR, superoxide reductase; 1Fe-SOR, SOR containing the [Fe(NHis)$_4$(SCys)] site as the only prosthetic group; 2Fe-SOR, SOR containing both the [Fe(NHis)$_4$(SCys)] and [Fe(SCys)$_4$] sites; 2Fe-SOR$_{pink}$, 2Fe-SOR containing ferric [Fe(SCys)$_4$] and ferrous [Fe(NHis)$_4$(SCys)] sites; 2Fe-SOR$_{gray}$, 2Fe-SOR containing ferric [Fe(SCys)$_4$] and ferric [Fe(NHis)$_4$(SCys)(Glu)] sites; E47A, engineered variant in which the glutamate ligand in the ferric [Fe(NHis)$_4$(SCys)(Glu)] site is replaced by an alanine residue; K48A, engineered variant in which lysine 48 is replaced by an alanine residue; C13S, engineered variant lacking the [Fe(SCys)$_4$] site; DTPA, diethylenetriaminepentaacetic acid; MES, 2-(*N*-morpholino)ethanesulfonic acid; HEPES, *N*-(2-hydroxyethyl)piperazine-*N*′-2-ethanesulfonic acid; TAPS, *N*-[tris(hydroxymethyl)methyl]-3-aminopropanesulfonic acid; CAPSO, 3-(cyclohexylamino)-2-hydroxy-1-propanesulfonic acid.

10.1021/bi700450u CCC: $37.00
Published on Web 09/14/2007

ligated "resting" ferric state (λ_{max} 645−650 nm). We proposed that the diffusion-controlled intermediate is a six-coordinate ferric−hydroperoxo complex. Formation of a spectroscopically identical diffusion-controlled intermediate has been verified for 1Fe- and 2Fe-SORs from other sources (*8*−*10*). An X-ray crystal structure of a hydrogen peroxide-reacted, mutated ferric SOR site (*11*) is consistent with our predicted end-on hydroperoxo coordination geometry for the 600 nm intermediate (*1*, *12*) and not with the sterically improbable, seven-coordinate side-on peroxo predicted by others (*13*−*15*). Whether superoxide reaction with the ferrous SOR site generates the same end-on-coordinated hydroperoxo remains to be established.

Our pulse radiolysis investigations also showed that replacement of the ferric-ligating glutamate by alanine (E47A) in the *D. vulgaris* 2Fe-SOR resulted in an identical 600 nm intermediate that decayed at the same rate as for the wild-type protein at and above neutral pH, but to a solvent- rather than glutamate-ligated resting ferric SOR site (*6*, *7*). The similar decay kinetics for the 600 nm intermediate in the wild-type and E47A 2Fe-SORs imply that decay of the putative ferric−hydroperoxo to the resting ferric site proceeds via rate-determining formation of a second species (bracketed in Scheme 1) that is rapidly scavenged by Glu47 coordination in the wild-type protein or solvent coordination in the E47A variant (*1*). The ferric-ligating glutamate residue is conserved in all known SORs and is part of a flexible polypeptide loop above the SOR site (*16*, *17*). This loop also contains an adjacent conserved lysine residue (Lys48 in *D. vulgaris* 2Fe-SOR) that sits above the ferrous SOR site and helps direct the negatively charged superoxide to the ferrous center. No other distinct species were observed between the 600 nm intermediate and resting ferric states in our pulse radiolysis studies of wild-type, E47A, K48A, or C13S *D. vulgaris* 2Fe-SOR.

In a subsequent pulse radiolysis investigation of the same recombinant *D. vulgaris* 2Fe-SOR studied by us, Nivière et al. reported that the 600 nm intermediate decayed to a second intermediate, which exhibited a relatively narrow absorption band with $\lambda_{max} \approx 625$ nm, and which apparently decayed to the resting ferric state (*18*). More recently, pulse radiolysis investigations of a 1Fe-SOR from the hyperthermophilic archaeon, *Archaeoglobus fulgidus*, found that the initial, diffusion-controlled intermediate decayed to a second intermediate whose pH-dependent absorption spectrum closely resembled that of ferric SOR sites in engineered variants lacking the ligating glutamate (*10*). The second intermediate observed in the native *A. fulgidus* 1Fe-SOR was, therefore, reasonably formulated as a six-coordinate solvent-ligated ferric species that decayed to the resting ferric site via displacement of solvent by the glutamate ligand. The second intermediate observed for the *A. fulgidus* 1Fe-SOR is clearly distinct from the second, pH-independent, narrow-absorption-band intermediate reported by Nivière et al.

All previously reported kinetics investigations of the SOR reaction have used pulse radiolysis to generate superoxide, which is only metastable and disproportionates in aqueous solutions near neutral pH. The pulse radiolysis method can rapidly generate reproducible, known quantities of superoxide such that its reactions can be readily monitored on the microsecond time scale. However, this method suffers from at least two restrictions (in addition to the limited availability of the instrumentation). First, radiolytic generation of superoxide involves production of high-energy electrons in aqueous solutions, which in the best-case scenario reduce dissolved dioxygen to superoxide. Second, pulse radiolysis cannot routinely generate higher than micromolar levels of aqueous superoxide. We have, therefore, developed a method to monitor the kinetics of SOR reactions with superoxide using stopped-flow spectrophotometry. Our stopped-flow method generates the putative ferric−hydroperoxo intermediate at much higher concentrations and at a much higher proportion of total SOR sites than has been reported for pulse radiolysis. Using the stopped-flow method, we have explored a wider range of experimental conditions and unresolved mechanistic issues, including identification of the transient question-marked species in Scheme 1 and its pathway of formation from the putative ferric−hydroperoxo intermediate.

MATERIALS AND METHODS

Reagents. Reagents and buffers were the highest grade commercially available. All solutions were prepared using water purified with a Milli-Q ultrapurification system (Millipore) to a resistivity of 18.2 MΩ to minimize contamination by trace metal ions. Deuterium oxide (99 atom % deuterium), DTPA, MES (pK_a = 6.1), HEPES (pK_a = 7.5), TAPS (pK_a = 8.4), CAPSO (pK_a = 9.6), potassium hexachloroiridate-(IV), and potassium superoxide were purchased from Sigma-Aldrich.

Preparation of 2Fe-SOR and Variants. The methods for expression, purification, and manipulation of recombinant *D. vulgaris* 2Fe-SOR$_{pink}$ and its E47A, K48A, and C13S variants and for active site concentration determinations have been described previously (*5*, *7*). 2Fe-SOR$_{gray}$ was prepared as described previously (*19*). Unless otherwise noted, experiments on the 2Fe-SOR variants were conducted identically to those described below for the wild-type protein.

Stopped-Flow Spectrophotometry. The kinetics of *D. vulgaris* 2Fe-SOR reactions were monitored using an SX 18MV or SX20 stopped-flow spectrophotometer (Applied Photophysics Ltd.) equipped with a photodiode array detector. Most of the data were collected on solutions maintained at 2−3 °C. For deuterium isotope effect experiments both the H_2O and D_2O solution data were collected at 12 °C (due to the higher freezing point of D_2O). Rate constants were determined by global component spectral fits using the Pro-K software package (Applied Photophysics Ltd.). The rate constants listed in the tables are averages and ranges of 3−5 replicate determinations.

Superoxide solutions were prepared immediately before use by dissolving 10−100 mg of solid potassium superoxide in 5 mL of degassed (to minimize dissolved carbon dioxide) aqueous solutions of 0.1 M NaOH and 0.5−2 mM DTPA. 2Fe-SOR$_{pink}$ solutions were prepared in 250 mM MES, pH 6, HEPES, pH 7, TAPS, pH 8−9, or CAPSO, pH 9.5−10.5, containing 0.5−2 mM DTPA. Since the ferrous SOR site does not autoxidize in air, the protein solutions were not degassed before use. The 2Fe-SOR$_{pink}$ and superoxide solutions were loaded into the 2.5 and 0.25 mL syringes, respectively, of the stopped-flow spectrophotometer. The 0.25 mL syringe and its corresponding flow circuit were flushed with 0.1 M NaOH and 0.5−2 mM DTPA prior to loading. Reactions were initiated by stopped-flow mixing

the 2Fe-SOR$_{pink}$ and superoxide solutions 10:1 (v/v) such that the concentrations immediately after mixing were in the range of 40−100 μM SOR sites and nominally 2.5−25 mM superoxide, based on the amount of solid KO_2 used. No more than 5 min elapsed between the time of preparation of the stock pH 13 KO_2 solutions and initiation of the stopped-flow mixing with the protein solutions. All spectral time courses were collected as difference spectra by referencing the spectrophotometer to the minimal absorbance changes occurring upon stopped-flow mixing of the same 2Fe-SOR$_{pink}$ stock solution 10:1 (v/v) against 0.1 M NaOH and 2 mM DTPA, i.e., the control solution without superoxide.

Deuterium solvent isotope effects were measured as described above on protein samples that had been exchanged into deuterated buffers by two 20-fold dilution/concentration cycles with either 250 mM HEPES, pD 7, or 250 mM TAPS, pD 8, in D_2O using Amicon Ultra-15 (10 000 MWCO) centrifugal filter devices (Millipore) at 5 °C. Potassium superoxide solutions were prepared as described above except substituting NaOD in place of NaOH. The 0.25 mL syringe and its flow circuit were flushed with 0.1 M NaOD and 2 mM DTPA prior to loading the deuterated superoxide solution. Similarly, the 2.5 mL syringe and its corresponding flow circuit were flushed with deuterated buffer prior to loading the deuterated protein solution.

RESULTS AND DISCUSSION

Ferrous SOR Site Oxidation by Superoxide Monitored by Stopped-Flow Spectrophotometry. Stopped-flow spectrophotometric experiments on superoxide dismutases have typically been conducted by premixing a dimethyl sulfoxide solution of potassium superoxide with a larger volume of water at a basic pH and then immediately combining this premix with the aqueous protein solution (*20*, *21*). While we have used this premix method successfully on SORs, we have found that a direct, entirely aqueous mixing method is more convenient and reproducible. The rate of disproportionation of superoxide in aqueous solution is strongly pH dependent. The second-order rate constants of 5.5×10^5 M^{-1} s^{-1} at pH 7 and 4.5 M^{-1} s^{-1} at pH 13 (*22*) translate to respective half-lives of a few milliseconds and several minutes for millimolar aqueous solutions of superoxide. We are aware of only one previous report where this basic pH stabilization of superoxide was exploited to directly stopped-flow mix aqueous superoxide with proteins, but the postmixing pH values were >9 (*23*). In our method, a freshly prepared stock solution of KO_2 in aqueous 0.1 M NaOH is directly stopped-flow mixed 1:10 (v/v) against a solution of 2Fe-SOR$_{pink}$ that is buffered sufficiently to neutralize the pH 13 superoxide solution; postmixing pH values as low as 6 are, thus, readily achieved.

On the basis of the previous pulse radiolysis results (*6*, *7*), formation of the putative ferric−hydroperoxo intermediate upon reaction of superoxide with the ferrous SOR site would be essentially complete within the stopped-flow mixing dead time, whereas decay of this intermediate occurs on a stopped-flow accessible time scale near room temperature and pH 6−9. The top panel of Figure 1 shows that stopped-flow spectrophotometry of the superoxide/2Fe-SOR$_{pink}$ reaction does indeed detect a single intermediate ($\lambda_{max} \approx 585$ nm) within the mixing dead time and its subsequent smooth decay to a final product spectrum ($\lambda_{max} \approx 645$ and 330 nm). The

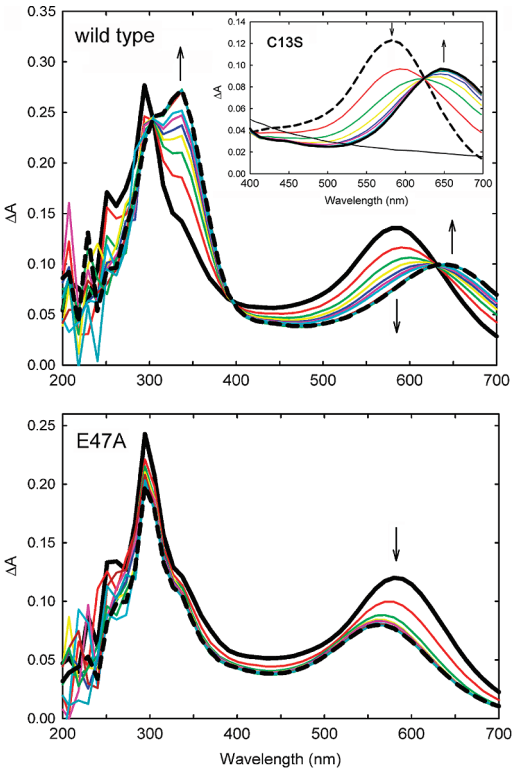

FIGURE 1: Difference absorption spectral time courses following stopped-flow mixing of *D. vulgaris* wild-type 2Fe-SOR$_{pink}$ (top panel), C13S 2Fe-SOR (top panel, inset), or E47A 2Fe-SOR$_{pink}$ (bottom panel) with pH 13 KO_2 solutions 10:1 (v/v), as described in the Materials and Methods. Conditions after mixing: 50 μM SOR sites, 20−25 mM KO_2 (nominal), either 250 mM TAPS, pH 8 (wild type and E47A), or 250 mM HEPES, pH 7.3 (C13S), 1 mM DTPA, 2 °C. For all the time courses, the solid and dashed black traces represent the first and last spectra obtained, respectively, and the variously colored traces were obtained at intermediate times. The first and last spectra were obtained, respectively, either 20 ms and 2 s (wild type, E47A) or 1 and 125 ms (C13S) after the mixing dead time. Arrows indicate directions of absorbance changes with time. The thin black trace in the top panel inset exemplifies the absolute spectra for the C13S 2Fe-SOR replicate time course without KO_2.

"dead time intermediate" spectrum is essentially identical to that assigned to the putative ferric−hydroperoxo intermediate detected by pulse radiolysis, and the final decay product spectrum is indistinguishable from that of the resting (Glu47-ligated) ferric SOR site (*19*). The [Fe(SCys)$_4$] site remains in the ferric state throughout the reaction, and its visible absorption spectrum partially overlaps that of the SOR site during the reaction with superoxide. For this reason, the spectral time courses are presented as difference absorption spectra (as was the case for the pulse radiolysis studies), in which a replicate stopped-flow time course in the absence of superoxide is subtracted from that in the presence of superoxide. C13S 2Fe-SOR contains the native ferrous SOR site but lacks the [Fe(SCys)$_4$] site and, prior to mixing with superoxide, shows no absorption features in the 400−700 nm region (*7*). The inset to the top panel of Figure 1 shows that the spectral time course for the C13S 2Fe-SOR stopped-flow reaction with superoxide is essentially identical to that obtained for the wild-type 2Fe-SOR$_{pink}$, with smooth decay of the dead time intermediate to the resting ferric SOR site. These spectral time courses are, thus, clearly monitoring reactions of the ferrous SOR site.

Table 1: Decay Rate Constants for the Stopped-Flow Dead Time Intermediate in the Reaction of *D. vulgaris* Wild-Type and Variant 2Fe-SOR$_{pink}$ with Superoxide[a]

protein	buffer, pH	k_{obs} (s^{-1})
wild type	MES, 5.5	>300[b]
	MES, 6.4	102 ± 2
	HEPES, 7.3	26 ± 6
	TAPS, 8	3.3 ± 0.5
	TAPS, 9	3.5 ± 0.3
C13S	HEPES, 7.3	43 ± 5
E47A	MES, 6.4	130 ± 13
	HEPES, 7.3	22 ± 2
	TAPS, 8	3 ± 1
K48A	MES, 6.4	300 ± 30
	HEPES, 7.3	147 ± 1
	TAPS, 8	6 ± 1

[a] For decay to the resting ferric SOR site following stopped-flow mixing with the pH 13 KO_2 solutions, as described in the Materials and Methods. Conditions after mixing: 250 mM concentration of the listed buffer + 1 mM DTPA at the listed pH, ~82 μM SOR sites, 20−25 mM (nominal) KO_2, temperature 2 °C. [b] The resting ferric SOR site spectrum formed within the mixing dead time with no subsequent spectral change. Therefore, only a lower limit for the decay k_{obs} can be estimated.

The clean isosbestic points at ~610 and ~400 nm for the wild-type 2Fe-SOR imply that no additional species accumulate between the dead time intermediate and the resting ferric SOR site. Consistent with this implication, global fittings of the spectral time courses yielded only two components, identical to the initial and final experimental spectra. The k_{obs} values listed in Table 1 were obtained from these global fits. The spectral time courses described above with smooth decay of the dead time intermediate to the resting ferric SOR site were obtained at all pH values listed in Table 1. The relative absorption intensities and λ_{max} values of the dead time intermediate and final product, as well as the decay kinetics, closely mimic our previously reported pulse radiolysis results (*6*, *7*). Analogous stopped-flow absorption spectral time courses revealed no detectable reaction of 2Fe-SOR$_{gray}$ with superoxide.

The bottom panel of Figure 1 shows that the same dead time intermediate spectrum is obtained for the E47A 2Fe-SOR$_{pink}$ reaction with KO_2. Figure 2 shows that the spectrum of the dead time intermediate decay product for the E47A variant is pH dependent in a manner identical to that of the solvent-ligated E47A ferric SOR site (*7*), which is reported to have a pK_a of 6.7 (*18*). A two-component fit was satisfactory at all pH values and gave decay k_{obs} values essentially indistinguishable from those for the wild-type 2Fe-SOR (Table 1). The spectral time courses shown in Figures 1 and 2 are, thus, *not* consistent with the dead time intermediate being a solvent-ligated ferric SOR site. The stopped-flow dead time intermediate and spectral time course for the K48A variant (see Figure S1 in the Supporting Information) closely resembled that for the wild-type protein, resulting in the resting ferric SOR site for this variant with no other detectable intermediates. These stopped-flow time courses are, thus, fully consistent with formulation of the dead time intermediate as a ferric-hydroperoxo which decays smoothly to the resting ferric SOR site.

A feature in the 330 nm region of the resting ferric SOR site absorption spectrum has been assigned to a mixture of ligand-to-metal charge-transfer transitions involving the His

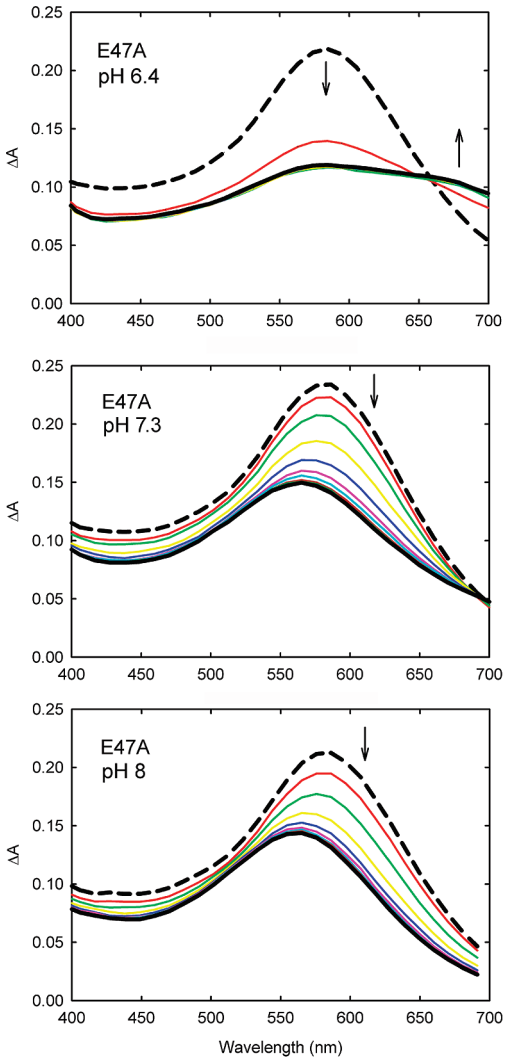

FIGURE 2: Difference absorption spectral time courses following stopped-flow mixing of *D. vulgaris* E47A 2Fe-SOR$_{pink}$ with pH 13 KO_2 solutions 10:1 (v/v). Conditions after mixing: buffer 250 mM MES, pH 6.4, HEPES, pH 7.3, or TAPS, pH 8, 82 μM SOR sites, 20−25 mM KO_2 (nominal), temperature 2 °C. For the pH 6.4 and 7.3 time courses, spectra are shown from 1 (dashed) to 100 (solid black) ms after the mixing dead time in 10 ms increments (variously colored). For the pH 8 time course, the corresponding times are 10−1000 ms in 100 ms increments. Arrows indicate directions of absorbance changes with time.

and possibly Cys and Glu ligands (*19*). Curiously, none of the previously published studies of SOR reactions with superoxide have reported the spectral time course below ~350 nm. The top panel of Figure 1 shows the buildup of a 330 nm absorption feature during decay of the dead time intermediate to the resting ferric SOR site. The 330 nm absorption also accumulates in the stopped-flow time course for the C13S variant (Figure S2 in the Supporting Information), demonstrating that this feature is not due to [Fe(SCys)$_4$] site absorption. The 330 nm absorption feature does not accumulate in the corresponding time courses for the E47A variant (Figure 1, bottom panel) or for the wild-type 2Fe-SOR in the presence of fluoride (Figure S2), which replaces the Glu47 ligand (see below). Glu47-to-ferric charge transfer, thus, appears to be a major contributor to the 330 nm feature of the wild-type resting ferric SOR site.

The concentration of SOR sites used for the results reported here ranged from 20 to 100 μM after stopped-flow

mixing. On the basis of the A_{585} of the dead time intermediate absorption spectrum and the extinction coefficient previously determined for the diffusion-controlled intermediate from pulse radiolysis (*6*), the dead time intermediate reproducibly exceeded 80% of the total SOR sites. Greater than 95% conversion was obtained using the final A_{645} and the corresponding extinction coefficient (1900 M^{-1} cm^{-1}) for the resting ferric SOR site (*7*). The yield of the intermediate and resting ferric state decreased as the SOR site concentration was increased to 200 μM, presumably reflecting an upper limit of the effective superoxide concentration in the stopped-flow reaction solutions. In any case both the concentrations of the dead time intermediate and the percentage conversion of total SOR sites were much higher using our stopped-flow method than achieved by pulse radiolysis, which invariably used substoichiometric superoxide (1−10 mol % of the SOR sites per pulse) (*7*, *10*, *18*).

To rule out participation of H_2O_2 in formation of the dead time intermediate, pH 13 solutions containing 100 mM H_2O_2 in place of KO_2 were stopped-flow mixed 1:10 (v/v) with pH 7.3 2Fe-SOR_{pink} solutions. This protocol gives a post-mixing H_2O_2 concentration of 9 mM, equivalent to that which would result if most of the superoxide in the corresponding pH 13 KO_2 solutions had disproportionated. The H_2O_2/2Fe-SOR_{pink} stopped-flow reaction mixtures showed no spectral evidence for significant oxidation (or any other reaction) of the ferrous SOR site on the time scale shown in Figure 1 (see Figure S3 in the Supporting Information). At longer reaction times (>30 s), the stopped-flow mixed H_2O_2/2Fe-SOR_{pink} solutions exhibited only smooth oxidation of the resting ferrous to resting ferric SOR site, which is consistent with our previous manual mixing results (*7*). As an additional probe of hydrogen peroxide effects, stopped-flow experiments were conducted in which wild-type and E47A 2Fe-SOR_{pink} solutions were premixed with a 6-fold molar excess of hydrogen peroxide in 250 mM TAPS, pH 8, and allowed to incubate for 500 ms prior to mixing 10:1 (v/v) with the pH 13 KO_2 solutions. These premix experiments showed unaltered time courses compared to control experiments in which H_2O_2 was omitted (see Figures S4 and S5 in the Supporting Information). *These stopped-flow spectral time courses, thus, monitor reactions of superoxide, not hydrogen peroxide, with the ferrous SOR site.*[2]

Effect of pH on Dead Time Intermediate Decay. The absorption spectrum of the dead time intermediate was found to be invariant from pH 5.5 to pH 10.5 (see Figure S6 in the Supporting Information). For the wild-type 2Fe-SOR the decay k_{obs} decreased between pH 5.5 and pH 8 and then became invariant from pH 8 to pH 9 (see Table 1). At pH 9.5 and above, the dead time intermediate decay k_{obs} may have increased somewhat, but this decay appeared to be convoluted with destruction of the SOR site, since the ultimate product retained no absorption in the 600−700 nm range. This pH dependence mimics that published in our previous pulse radiolysis study (*7*). The decay k_{obs} was found to be approximately first order in $[H^+]$ from pH 5.5 to pH 7, consistent with a single diffusion-controlled protonation by H_3O^+, and invariant between pH 8 and pH 9.5, consistent with rate-limiting protonation of the intermediate by solvent. The pH dependences of the decay k_{obs} for the E47A and K48A variants paralleled those for the wild-type protein (Table 1); the K48A variant showed a modestly higher decay k_{obs} at the three pH values investigated (Table 1) relative to that of the wild-type or E47A protein.

Three different aminosulfonate buffers (MES, HEPES, TAPS), as well as several other amino buffers, had little or no effect on the decay rate of the dead time intermediate at pH 7 or 8 (see Table S1 in the Supporting Information). The pH dependence of the decay k_{obs} is, thus, not due to the nature of these amino buffers. As for our earlier pulse radiolysis experiments on *D. vulgaris* 2Fe-SOR (*7*), the stopped-flow time courses showed *no evidence for any other intermediates following the dead time intermediate at any of the pH values tested for either the wild-type or alanine variant 2Fe-SOR.*

Effects of Added Anions. Large excesses of azide are known to form complexes with the resting ferrous and ferric SOR sites, displacing the ligating glutamate in the ferric site (*24*). However, the effects of exogenous anions on the kinetics of the ferrous SOR site reaction with superoxide have not been examined. The spectrum of the dead time intermediate was unaffected by ≥500-fold molar excesses over SOR sites of chloride, fluoride, azide, formate, phosphate, or carbonate in the buffered 2Fe-SOR_{pink} solutions that were stopped-flow mixed with the pH 13 KO_2 solutions. No effect on the dead time intermediate decay rate was observed in the presence of excess chloride (100−500 mM) or carbonate (50 mM). The decay rate was, however, significantly faster in the presence of excess azide, fluoride, phosphate, or formate (see Tables 2 and 3). As shown in Figure 3 and listed in Table 2, at pH 7 and <50 mM azide, the dead time intermediate decayed in an $[N_3^-]$-dependent process to a more intensely absorbing species ($\lambda_{max} \approx 635$ nm), which then decayed in a slower $[N_3^-]$-independent process to the resting ferric state. Independent spectrophotometric titrations of 2Fe-SOR_{gray} verified that the $\lambda_{max} \approx$ 635 nm species is the ferric−azido SOR site (see Figure S7 in the Supporting Information). At pH 8 and >10 mM azide, the dead time intermediate decayed to the azide adduct with no evidence for any other intermediate or product (see Figure 3). Similarly, in the presence of 50 mM fluoride at pH 7, the dead time intermediate decayed apparently directly to a final, weaker absorbing species with $\lambda_{max} \approx 570$ nm (see Figures 3 and S2), which spectral titrations (Figure S7) identified as the ferric−fluoro SOR site.[3] Thus, in the presence of excess azide or fluoride, the dead time intermediate decayed initially to the ferric−azido or ferric−fluoro complex, respectively. In the vicinity of the K_d values for binding of azide (25 mM) and fluoride (1.9 mM) (see Figure S7) to the wild-type ferric SOR site, mixtures of the anion adducts and resting ferric SOR sites were obtained as the products of dead time intermediate decay. The decay rates increased with increasing azide or fluoride concentrations,

[2] These stopped-flow measurements, by themselves, do not rule out formation of the ferric−hydroperoxo intermediate via a mechanism in which outer-sphere oxidation of the ferrous SOR site by superoxide produces an initial five-coordinate ferric SOR site that rapidly reacts with hydrogen peroxide (arising from "spontaneous" superoxide disproportionation). However, given the diffusion-controlled formation of the intermediate previously established by pulse radiolysis, such a two-step mechanism seems unlikely.

[3] A similarly absorbing ferric−fluoro SOR site was reported for *A. fulgidus* 1Fe-SOR (*10*), but the effect of fluoride on reaction of the ferrous SOR site with superoxide was not reported.

Table 2: Anion Effects on Decay of the Stopped-Flow Dead Time Intermediate for Reaction of Wild-Type *D. vulgaris* 2Fe-SOR_{pink} with Superoxide[a]

anion/ concn (mM)	k_{obs} (s^{-1})	SOR site concn (μM)	anion/ concn (mM)	k_{obs} (s^{-1})	SOR site concn (μM)
azide/50	290 ± 50[b]	41	formate/100	143 ± 5	77
azide/10	180 ± 30,[c] 12 ± 1[d]	50	control	26 ± 3	77
control	23 ± 2	41	phosphate/50[f]	20 ± 4	90
fluoride/50	80 ± 1[e]	92	control[f]	3.4 ± 0.8	90
control	33.8 ± 0.2	92	phosphate/100[g]	60 ± 8	90

[a] Anions, as sodium salts, were added to the 2Fe-SOR_{pink} solutions prior to their stopped-flow mixing with the pH 13 KO_2 solutions 10:1 (v/v), as described in the Materials and Methods with 20−25 mM (nominal) KO_2 immediately after mixing. All other listed concentrations were after mixing. Control experiments were replicates, but omitting the added anion. Unless otherwise noted, the buffer was 250 mM HEPES, 1 mM DTPA, pH 7.3, the temperature was 2 °C, and the decay product was the resting ferric SOR site. [b] For decay to a mixture of the ferric−azido and resting ferric SOR sites. [c] For decay to the ferric−azido SOR site. [d] For decay of the ferric−azido to the resting ferric SOR site. [e] For decay to the ferric−fluoro SOR site. [f] The buffer was 250 mM TAPS, 50 mM phosphate, 1 mM DTPA, pH 8, or for the control 300 mM TAPS, 1 mM DTPA, pH 8. [g] The buffer was 100 mM phosphate, pH 7, 0.1 mM DTPA (no other buffer components).

Table 3: Solvent Deuterium Isotope Effects on Decay of the Stopped-Flow Dead Time Intermediate in Reactions of *D. vulgaris* 2Fe-SOR_{pink} with Superoxide

protein	conditions[a]	k_{obs} (s^{-1})	$k_{obs,H_2O}/k_{obs,D_2O}$
wild type	pH 7	71 ± 6	
	pD 7	34 ± 1	2.1 ± 0.2
	pH 8	7.8 ± 0.7	
	pD 8	3.0 ± 0.4	2.6 ± 0.4
	pH 8 + 25 mM azide	53 ± 7[b]	
	pD 8 + 25 mM azide	23 ± 5[b]	2.3 ± 0.6
E47A	pH 8	8 ± 1	
	pD 8	2.4 ± 0.3	3.3 ± 0.6
K48A	pH 8	30 ± 3	
	pD 8	14 ± 3	2.1 ± 0.5

[a] Postmixing conditions: buffer 250 mM HEPES, 2 mM DTPA, pH/D 7, or 250 mM TAPS, 2 mM DTPA, pH/D 8, SOR site concentration 50 μM (wild type and E47A) or 92 μM (K48A), 20−25 mM KO_2 (nominal), temperature 12 °C. [b] For decay to the ferric−azido SOR site.

but the dependence was less than first order (see below).

The ~5-fold acceleration in dead time intermediate decay induced by 100 mM formate (Table 2) is noteworthy because formate at this concentration has been used to convert hydroxyl radicals to superoxide in some pulse radiolysis studies of 2Fe-SORs (*8*, *18*).[4] In the presence of excess formate at pH 8 the E47A ferric SOR site has an absorption spectrum (not shown) closely resembling that of the wild-type resting ferric SOR site ($\lambda_{max} \approx 645$ nm), as expected for carboxylate coordination in both cases. We, therefore, cannot spectrally distinguish endogenous from exogenous carboxylate ligation. Despite the ~6-fold increase in the dead time intermediate decay k_{obs} in the presence of 50 mM phosphate at pH 8 or 100 mM phosphate at pH 7 (see Table 2), the spectrally distinctive ferric−phosphato SOR site (*10*) was not detected.

Specific- and General-Acid Catalysis. Solvent deuterium isotope effects support both specific- and general-acid contributions to decay of the dead time intermediate. A solvent deuterium isotope effect on decay (but not on formation) of the putative ferric−hydroperoxo intermediate at pH 8 of ~2 was reported for the wild-type 2Fe-SOR in our previous pulse radiolysis study (*7*). A more extensive investigation of this effect was conducted using our stopped-flow method. The results are summarized in Table 3. A solvent deuterium isotope effect, $k_{obs,H_2O}/k_{obs,D_2O} \geq 2$, was observed for decay of the dead time intermediate following stopped-flow mixing of the wild-type 2Fe-SOR_{pink} with superoxide at both pH 7 and pH 8. Proton transfer must, therefore, occur during the rate-determining step of the decay process at both pH values. Similar solvent deuterium isotope effects on dead time intermediate decay were observed for the corresponding E47A and K48A variants (see Table 2), indicating that neither of these conserved residues is required for rate-determining proton donation. Together with the absence of significant contributions from the various amino buffers, these deuterium isotope effects support direct proton transfer from solvent as the rate-determining step in dead time intermediate decay. A solvent deuterium isotope effect was also observed at pH 8 for the ~8-fold faster decay rate induced by 25 mM azide (Table 2), indicating that azide lowers the activation barrier for proton transfer, presumably via its protonated form. Consistent with this interpretation, the decay k_{obs} was found to be directly proportional to $[HN_3]$, as shown in Figure 4. No evidence for saturation (i.e., leveling off of k_{obs}) was observed up to 500 mM total azide at pH 8. Parameters obtained from fitting of the equation $k_{obs} = k_{H_2O} + k_{HN_3}[HN_3]$ to the data in Figure 4 are listed in Table 4. Corresponding plots for fluoride and formate are contained in Figure S8 in the Supporting Information, and data from those fits are included in Table 4. Sodium chloride at up to 500 mM had no effect on the decay k_{obs}, indicating that the [HX] dependences listed in Table 4 are not salt effects. From the pH dependence of k_{obs} (Table 1), a $k_{H_3O^+}$ of 10^9 M^{-1} s^{-1} can be estimated; this value is consistent with that reported in our pulse radiolysis study (*7*).

Summary, Conclusions, and Context. On the basis of our stopped-flow kinetics results for the reaction of *D. vulgaris* 2Fe-SOR_{pink} with superoxide, we conclude the following: (i) the putative ferric−hydroperoxo intermediate previously observed by pulse radiolysis is obtained as the dead time intermediate in the stopped-flow time courses; (ii) this dead time intermediate is due to reaction of superoxide, not hydrogen peroxide, with the ferrous SOR site; (iii) the dead time intermediate decays smoothly to the resting ferric SOR site at ~30 s^{-1} (at 2 °C and pH 7) *with no other detectable intermediates*; (iv) solvent acts as a specific acid in the rate-determining step of dead time intermediate decay; (v) neither the ferric SOR site ligand, Glu47, nor the pocket residue, Lys48, functions as a proton donor in the rate-determining

[4] Our previously reported pulse radiolysis studies on *D. vulgaris* 2Fe-SOR (*7*) used formate at only 10 mM and pH 8, which induced much more modest increases in the intermediate decay rates.

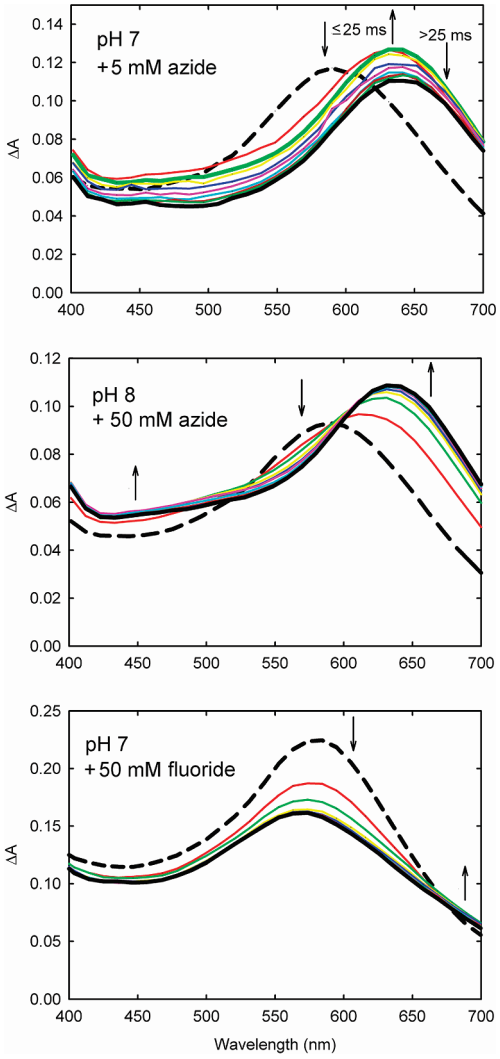

FIGURE 3: Difference absorption spectral time courses following stopped-flow mixing of *D. vulgaris* wild-type 2Fe-SOR$_{pink}$ containing excess azide or fluoride with pH 13 KO_2 solutions 10:1 (v/v). Conditions after mixing: 250 mM HEPES, pH 7.3, or 250 mM TAPS, pH 8, 20−25 mM KO_2 (nominal), 50 μM SOR sites + either 5 or 50 mM NaN_3 or 90 μM SOR sites + 50 mM NaF, temperature 2 °C. Time courses are depicted as the first spectra collected after the mixing dead time (dashed), subsequent spectra (variously colored), and last spectra collected (solid black). The pH 7 + azide or fluoride spectra are displayed in 10 ms increments starting 1 ms and ending 115 ms after the mixing dead time. The green trace in the pH 7 + azide panel was collected at 25 ms (maximal $A_{635\ nm}$). The pH 8 + azide spectra are displayed in 20 ms increments from 20 to 120 ms (purple trace) and at longer subsequent intervals ending 2 s after the mixing dead time. Arrows indicate directions of absorbance changes with time.

step of dead time intermediate decay; (vi) the protonated forms of several exogenous anions mimic the solvent as general acids, thereby accelerating decay of the dead time intermediate. The question-marked transient species in Scheme 1 is, thus, formulated as the anion-ligated ferric SOR site shown in Scheme 2, which summarizes our key results and conclusions.

Nivière et al. reported that pulse radiolysis on the same *D. vulgaris* 2Fe-SOR used by us resulted in formation of a second intermediate via first-order decay of the diffusion-controlled intermediate at ~420 s^{-1}; this second intermediate apparently decayed to the resting ferric state at <5 s^{-1} (pH 7.6 and 20 °C), although the latter time course could not be

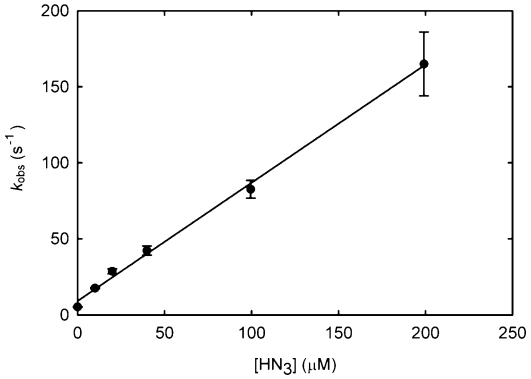

FIGURE 4: Dependence of k_{obs} for dead time intermediate decay on [HN_3]. Conditions immediately after stopped-flow mixing: 250 mM TAPS, 5 mM DTPA, pH 8, 45 μM SOR sites, 2.5 mM (nominal) KO_2, 0−500 mM NaN_3, temperature 3 °C. The decay product was the azido−ferric SOR site for all but the zero azide data point.

Table 4: Fitted First- and Second-Order Rate Constants for General- and Specific-Acid Catalysis of Dead Time Intermediate Decay upon Reaction of KO_2 with *D. vulgaris* 2Fe-SOR$_{pink}$[a]

HX	pK_a	k_{H_2O} (s^{-1})	k_{HX} (10^6 M^{-1} s^{-1})
HF	3.15	6.1 ± 0.4	3.6 ± 0.2
HCOOH	3.75	8 ± 1	1.4 ± 0.8
HN_3	4.60	9 ± 2	0.80 ± 0.02

[a] Postmixing conditions: 250 mM TAPS, 5 mM DTPA, pH 8, ~40 μM SOR sites, 2.5 mM (nominal) KO_2, temperature 2−3 °C.

Scheme 2

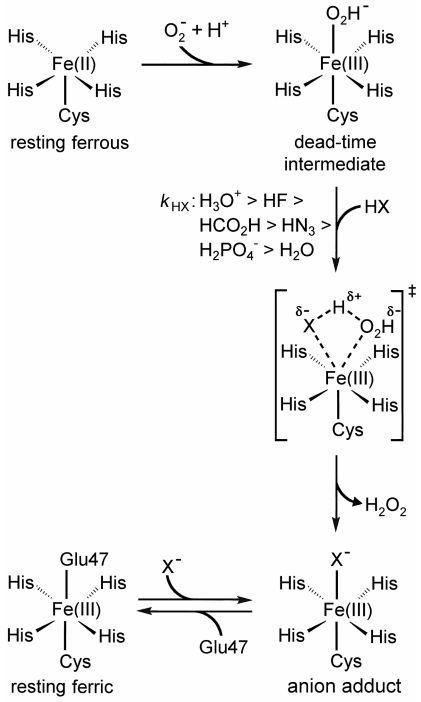

measured with their spectrometer (*18*). On the basis of these time scales, our dead time intermediate could conceivably be the second intermediate observed by Nivière et al. However, the reported absorption spectral properties (narrow bandwidth, λ_{max} 625 nm, $\epsilon_{625\ nm}$ 3000 M^{-1} cm^{-1}) of Nivière et al.'s second intermediate do not match those of our dead time intermediate for the *D. vulgaris* wild-type, C13S, E47A, or K48A 2Fe-SOR between pH 5.5 and pH 10.5 or in the

presence of various anions. They also do not match those of the single intermediate we observed in our previous pulse radiolysis studies under a similarly wide range of conditions (*7*). We choose not to speculate about the reason(s) for these discrepancies but simply note that our results are highly reproducible.

The same pH dependences and deuterium isotope effects on the rates of dead time intermediate decay are observed for the wild-type, E47A, and K48A 2Fe-SORs, supporting direct solvent delivery of protons in the rate-determining step. Retention of the solvent deuterium isotope effect in the azide-accelerated decay of the dead time intermediate and the first-order dependence of the decay k_{obs} on $[HN_3]$ support a general-acid mechanism involving the exogenous protonated anions, even at pH values 3 orders of magnitude above their pK_a values. The decrease of the fitted second-order rate constants, k_{HX}, with increasing pK_a of HX listed in Table 4 is the trend expected from the Brønsted catalysis law. The estimate of 10^9 M^{-1} s^{-1} for the corresponding $k_{H_3O^+}$ is consistent with this trend (p$K_a(H_3O^+) = -1.7$). The clear implication of our results is that the protonated anions mimic solvent in rate-determining protonation of the dead time intermediate. In the proposed transition state shown in Scheme 2, HX donates a proton to the iron-bound oxygen of the ferric−hydroperoxo. X^- then either displaces the incipient H_2O_2 concertedly with the proton transfer or coordinates to the ferric center rapidly following dissociation of hydrogen peroxide. Our computational study (*12*) indicated that a ferric−hydrogen peroxide complex has no energy minimum, i.e., that it would not be a transient intermediate following proton transfer from HX.

Consistent with this mechanistic analysis, ferric−azido or ferric−fluoro SOR sites are the observed decay products of the dead time intermediate in the presence of excess azide or fluoride. The position of the equilibrium between the X^-- and Glu47-ligated forms in Scheme 2 is dependent on the nature of the anion and pH. Azide and fluoride adducts clearly form at >10 mM anion in the pH 6−8 range. In the pH 6−9 range, no spectral evidence was observed for the phosphato adduct during or following dead time intermediate decay. Manual titrations of the wild-type 2Fe-SOR_{gray} indicated that the phosphate K_d for the resting ferric SOR site exceeds 500 mM at pH 7−8 (Huang, V. W., and Kurtz, D. M., Jr., unpublished results). For the wild type 2Fe-SOR_{pink} reaction with superoxide, the spectrally distinctive hydroxo adduct became evident as a decay product only at pH ≥ 9. However, for the E47A 2Fe-SOR_{pink} reaction with superoxide at neutral pH, the hydroxo adduct is the only observed product of dead time intermediate decay. Similarly, phosphate at 50 mM forms an adduct with the resting ferric SOR site of the E47A 2Fe-SOR. According to the mechanism shown in Scheme 2, Glu47 in *D. vulgaris* 2Fe-SOR must, therefore, rapidly displace hydroxo (below pH 9) and phosphato ligands from the ferric SOR site produced upon loss of hydrogen peroxide. At least in the case of hydroxo this last step is solvent proton driven, on the basis of the resting ferric SOR site pK_a of 9 for interconversion with the hydroxo-ligated form (*18*). It is not immediately obvious why formate accelerates decay of the dead time intermediate while the endogenous carboxylate from Glu47 does not (on the basis of the similar dead time intermediate decay rates for wild-type and E47A 2Fe-SORs). The (nonligated) surface-exposed Glu47 carboxylic acid is expected to have a pK_a within or near the range of those of HCOOH (3.7) and HN_3 (4.6). Conformational and/or steric features of the local environment could conceivably inhibit formation of a transition state with the protonated Glu47 analogous to that shown in Scheme 2 for HX.

Katona et al. (*11*) have recently emphasized a catalytic role for Lys48 in protonation of the ferric−hydroperoxo intermediate. Our results contradict this assertion and suggest that Lys48 may even slightly inhibit decay of the ferric−hydroperoxo intermediate (see Table 1). The general-acid catalysis discussed above and the relatively high pK_a (∼10) of lysine ϵ-ammonium groups in proteins explain why Lys48 does not function as an efficient proton donor to the intermediate. The absence of significant general-acid catalysis by the aminosulfonate buffers can also be attributed to their relatively high pK_a values and/or steric hindrance caused by the large substituents on these secondary and tertiary amines. Finally, the observation that excess hydrogen peroxide does not accelerate decay of the dead time intermediate is consistent with its relatively high pK_a (11.6) and consequent inability to function as a general acid.

Pulse radiolysis studies of *A. fulgidus* 1Fe-SOR showed that the diffusion-controlled intermediate decayed first to the hydroxo-ligated ferric SOR site and then to the resting (glutamate-ligated) ferric SOR site at pH 7 (*10*). As for the *D. vulgaris* 2Fe-SOR, excess phosphate accelerated decay of the diffusion-controlled intermediate in *A. fulgidus* 1Fe-SOR, presumably via proton donation. However, in contrast to the *D. vulgaris* 2Fe-SOR, a phosphato−ferric SOR site was reported as the initial decay product in *A. fulgidus* 1Fe-SOR, and phosphate actually slowed conversion to the resting (glutamate-ligated) ferric SOR site. Thus, the glutamate corresponding to Glu47 in *D. vulgaris* 2Fe-SOR does not so readily compete with hydroxo and phosphato ligands in the *A. fulgidus* 1Fe-SOR. This contrasting behavior has been suggested to be due to the hyperthermophilic *A. fulgidus* producing an SOR that is relatively conformationally rigid near room temperature, where the pulse radiolysis was conducted (*10*). One source of local rigidity may be a hydrogen bond between the glutamate carboxylate and Nδ of a His ligand at the ferrous site of SORs from hyperthermophiles (*10*, *17*). This interaction has not been observed in 2Fe-SORs from mesophiles (*11*, *16*, *25*).

Among the anions found to have an effect on decay of the putative ferric−hydroperoxo intermediate, only phosphate is likely to be universally present in vivo at concentrations sufficient to potentially affect the SOR catalytic cycle. The phosphate-induced acceleration of the dead time intermediate decay to the resting ferric SOR site without apparent formation of a ferric−phosphato SOR site confirms our previous analysis of the *D. vulgaris* 2Fe-SOR catalytic cycle, which was conducted in phosphate buffer (*26*).[5] Decay of the putative ferric−hydroperoxo intermediate is, thus, not rate-limiting for turnover, nor is re-reduction of the ferric SOR site. At the typical nanomolar or lower steady-state assay (and intracellular) superoxide concentrations, the turnover-limiting step is most likely the diffusion-controlled

[5] Our analysis of the SOR catalytic cycle (*26*) has been questioned (*10*) because it was based on rate constants for intermediate decay that had been measured in the absence of phosphate.

encounter of superoxide with the ferrous SOR site. Notably, the *D. vulgaris* E47A 2Fe-SOR in 50 mM phosphate buffer showed well-coupled SOR turnover activity essentially indistinguishable from that of the wild-type protein (*26*). Glu47 must, therefore, not be required for inhibition of phosphate binding to the ferric SOR site during turnover, nor does premixing with hydrogen peroxide affect the E47A ferrous SOR site's stopped-flow reaction with superoxide (see Figure S5). Previous studies have established that the E47A substitution does not induce significant superoxide dismutase activity (*1*). The reason for the apparently strict conservation of this ferric SOR site glutamate ligand, thus, remains mysterious.

The stopped-flow kinetics of the ferrous SOR site oxidation by the outer-sphere oxidant hexachloroiridate(IV) are instructive when compared with those of superoxide, particularly since these two oxidants have very similar redox potentials. Hexachloroiridate(IV) oxidation of the ferrous SOR site in *A. fulgidus* 1Fe-SOR resulted in the hydroxo-ligated ferric SOR site as the initial (dead time) product, which then decayed to the resting (glutamate-ligated) ferric SOR site (*10*). The analogous hexachloroiridate(IV) oxidation of *D. vulgaris* 2Fe-SOR_{pink} showed the resting (Glu47-ligated) ferric SOR site forming within the stopped-flow mixing dead time and no further reaction (Huang, V. W., and Kurtz, D. M., Jr., unpublished results). Presumably, the rapid outer-sphere hexachloroiridate(IV) oxidation produces a transient five-coordinate ferric SOR site that is rapidly scavenged by either solvent (in *A. fulgidus* 1Fe-SOR) or Glu47 (in *D. vulgaris* 2Fe-SOR) coordination. These consequences of outer-sphere oxidation are clearly distinct from those arising from superoxide oxidation of the SOR site, consistent with an inner-sphere process in the latter case. That is, the diffusion-controlled ferric intermediate arising from reaction of the ferrous SOR site with superoxide has the sixth coordination position occupied by an exogenous ligand directly derived from superoxide, which inhibits coordination of Glu47 as well as solvent and exogenous anions. Our results, thus, support the notion that reaction of the ferrous SOR site with superoxide leads directly to a ferric−hydroperoxo intermediate, the decay of which is subject to both specific- and general-acid catalysis.

ACKNOWLEDGMENT

This paper is dedicated to the fond memory of Eric Coulter. We thank Professor Robert Phillips for allowing J.P.E. to conduct some preliminary stopped-flow experiments at the University of Georgia.

SUPPORTING INFORMATION AVAILABLE

Experimental descriptions and figures for stopped-flow absorption spectral time courses for reactions of K48A, C13S, and [wild type + fluoride] 2Fe-SOR_{pink} with KO_2 and wild-type 2Fe-SOR_{pink} with hydrogen peroxide, premix reactions of wild-type and E47A 2Fe-SOR_{pink} with hydrogen peroxide and superoxide, dead time intermediate UV−vis absorption spectra from pH 5.5 to pH 10.5, UV−vis absorption spectral titrations of 2Fe-SOR_{gray} with azide and fluoride, and the dependence of k_{obs} on [HF] and [HCOOH] and tables listing dead time intermediate decay k_{obs} in various buffers and at various azide and fluoride concentrations. This material is available free of charge via the Internet at http://pubs.acs.org.

REFERENCES

1. Kurtz, D. M., Jr. (2004) Microbial detoxification of superoxide: The non-heme iron reductive paradigm for combating oxidative stress, *Acc. Chem. Res. 37*, 902−908.
2. Kurtz, D. M., Jr. (2006) Avoiding high-valent iron intermediates: superoxide reductase and rubrerythrin, *J. Inorg. Biochem. 100*, 679−693.
3. Nivière, V., and Fontecave, M. (2004) Superoxide reductase: an historical perspective, *J. Biol. Inorg. Chem. 9*, 119−123.
4. Adams, M. W. W., Jenney, F. E., Jr., Clay, M. D., and Johnson, M. K. (2002) Superoxide reductase: fact or fiction? *J. Biol. Inorg. Chem. 7*, 647−652.
5. Emerson, J. P., Cabelli, D. E., and Kurtz, D. M., Jr. (2003) An engineered two-iron superoxide reductase lacking the [$Fe(SCys)_4$] site retains its catalytic properties in vitro and in vivo, *Proc. Natl. Acad. Sci. U.S.A. 100*, 3802−3807.
6. Coulter, E. D., Emerson, J. P., Kurtz, D. M., Jr., and Cabelli, D. E. (2000) Superoxide reactivity of rubredoxin oxidoreductase (desulfoferrodoxin) from *Desulfovibrio vulgaris*: a pulse radiolysis study, *J. Am. Chem. Soc. 122*, 11555−11556.
7. Emerson, J. P., Coulter, E. D., Cabelli, D. E., Phillips, R. S., and Kurtz, D. M., Jr. (2002) Kinetics and mechanism of superoxide reduction by two-iron superoxide reductase from *Desulfovibrio vulgaris*, *Biochemistry 41*, 4348−4357.
8. Lombard, M., Houée-Levin, C., Touati, D., Fontecave, M., and Nivière, V. (2001) Superoxide reductase from *Desulfoarculus baarsii*: reaction mechanism and role of glutamate 47 and lysine 48 in catalysis, *Biochemistry 40*, 5032−5040.
9. Nivière, V., Lombard, M., Fontecave, M., and Houée-Levin, C. (2001) Pulse radiolysis studies on superoxide reductase from *Treponema pallidum*, *FEBS Lett. 497*, 171−173.
10. Rodrigues, J. V., Abreu, I. A., Cabelli, D., and Teixeira, M. (2006) Superoxide reduction mechanism of *Archaeoglobus fulgidus* one-iron superoxide reductase, *Biochemistry 45*, 9266−9278.
11. Katona, G., Carpentier, P., Nivière, V., Amara, P., Adam, V., Ohana, J., Tsanov, N., and Bourgeois, D. (2007) Raman-assisted crystallography reveals end-on peroxide intermediates in a non-heme iron enzyme, *Science 316*, 449−453.
12. Silaghi-Dumitrescu, R., Silaghi-Dumitrescu, I., Coulter, E. D., and Kurtz, D. M., Jr. (2003) Computational study of the non-heme iron active site in superoxide reductase and its reaction with superoxide, *Inorg. Chem. 42*, 446−456.
13. Mathé, C., Mattioli, T. A., Horner, O., Lombard, M., Latour, J.-M., Fontecave, M., and Nivière, V. (2002) Identification of an iron(III) peroxo species in the active site of superoxide reductase from *Desulfoarculus baarsii*, *J. Am. Chem. Soc. 124*, 4966−4967.
14. Horner, O., Mouesca, J. M., Oddou, J. L., Jeandey, C., Nivière, V., Mattioli, T. A., Mathé, C., Fontecave, M., Maldivi, P., Bonville, P., Halfen, J. A., and Latour, J. M. (2004) Mössbauer characterization of an unusual high-spin side-on peroxo-Fe^{3+} species in the active site of superoxide reductase from *Desulfoarculus baarsii*. Density functional calculations on related models, *Biochemistry 43*, 8815−8825.
15. Mathé, C., Nivière, V., Houée-Levin, C., and Mattioli, T. A. (2005) $Fe^{3+}-\eta^2$−peroxo species in superoxide reductase from *Treponema pallidum*. Comparison with *Desulfoarculus baarsii*, *Biophys. Chem. 118*, 98−108.
16. Coehlo, A. V., Matias, P., Fülop, V., Thomson, A., Gonzalez, A., and Carrondo, M. A. (1997) Desulfoferrodoxin structure determined by MAD phasing and refinement to 1.9-Å reveals a unique combination of a tetrahedral FeS_4 centre with a square pyramidal $FeSN_4$ centre, *J. Biol. Inorg. Chem. 2*, 680−689.
17. Yeh, A. P., Hu, Y., Jenney, F. E., Jr., Adams, M. W., and Rees, D. C. (2000) Structures of the superoxide reductase from *Pyrococcus furiosus* in the oxidized and reduced states, *Biochemistry 39*, 2499−508.
18. Nivière, V., Asso, M., Weill, C. O., Lombard, M., Guigliarelli, B., Favaudon, V., and Houée-Levin, C. (2004) Superoxide reductase from *Desulfoarculus baarsii*: identification of protonation steps in the enzymatic mechanism, *Biochemistry 43*, 808−818.
19. Clay, M. D., Emerson, J. P., Coulter, E. D., Kurtz, D. M., Jr., and Johnson, M. K. (2003) Spectroscopic characterization of the [$Fe(His)_4(Cys)$] site in 2Fe-superoxide reductase from *Desulfovibrio vulgaris*, *J. Biol. Inorg. Chem. 8*, 671−82.

20. Bull, C., and Fee, J. A. (1985) Steady-state kinetic studies of superoxide dismutases: properties of the iron-containing protein from *Escherichia coli*, *J. Am. Chem. Soc. 107*, 3295−3304.
21. Greenleaf, W. B., and Silverman, D. N. (2002) Activation of the proton transfer pathway in catalysis by iron superoxide dismutase, *J. Biol. Chem. 277*, 49282−49826.
22. Bielski, B. H. J., Cabelli, D. E., and Arudi, R. L. (1985) Reactivity of HO_2/O_2^- radicals in aqueous solution, *J. Phys. Chem. Ref. Data 14*, 1041−1100.
23. Bradic, Z., and Wilkins, R. G. (1984) Comparative behavior in the kinetics of reduction by superoxide and dithionite ions, *J. Am. Chem. Soc. 106*, 2236−2239.
24. Clay, M. D., Jenney, F. E., Jr., Hagedoorn, P. L., George, G. N., Adams, M. W. W., and Johnson, M. K. (2002) Spectroscopic studies of *Pyrococcus furiosus* superoxide reductase: implications for active-site structures and the catalytic mechanism, *J. Am. Chem. Soc. 124*, 788−805.
25. Berthomieu, C., Dupeyrat, F., Fontecave, M., Vermeglio, A., and Nivière, V. (2002) Redox-dependent structural changes in the superoxide reductase from *Desulfoarculus baarsii* and *Treponema pallidum*: a FTIR study, *Biochemistry 41*, 10360−10368.
26. Emerson, J. P., Coulter, E. D., Phillips, R. S., and Kurtz, D. M., Jr. (2003) Kinetics of the superoxide reductase catalytic cycle, *J. Biol. Chem. 278*, 39662−39668.

BI700450U